A Highly Efficient Coordination Polymer for Selective Trapping and Sensing Perrhenate/Pertechnetate

Cheng-Peng Li,[†,‡] Hang Zhou,[†] Jing Chen,[†] Jia-Jun Wang,[†] Miao Du*[,†] and Wuzong Zhou*[,‡]

[†] *Tianjin Key Laboratory of Structure and Performance for Functional Molecules, MOE Key Laboratory of Inorganic–Organic Hybrid Functional Material Chemistry, College of Chemistry, Tianjin Normal University, Tianjin 300387, P. R. China*

[‡] *School of Chemistry, University of St Andrews, St Andrews, Fife KY169ST, UK*

Keywords: Coordination Polymers; Perrhenate/Pertechnetate; Anion Exchange; Fluorescence Sensor; Test Paper

ABSTRACT

A porous cationic Ag(I) coordination polymer, [Ag(1,2,4,5-p4b)](SbF_6) (TJNU-302) with the ligand 1,2,4,5-p4b (1,2,4,5-tetra(pyridin-4-yl)benzene), is reported, which shows high sorption capacity (211 mg g^{-1}) and distribution coefficient K_d (5.8×10^5 mL g^{-1}) as well as outstanding selectivity in 500 times excess of CO_3^{2-} or PO_4^{3-} anion for perrhenate removal. TJNU-302 can act as a crystalline turn-off sensor for perrhenate upon UV radiation. In this way, a test paper strip for sensing ReO_4^- could be produced. In water solution, TJNU-302 shows efficient fluorescence quenching response to ReO_4^- ion, with the highest quenching percentage (86%) among all reported ReO_4^- sensors. These results could be elucidated by the bonding properties of single-crystal structures of TJNU-302 before and after perrhenate sorption, as well as density functional theory (DFT) calculations.

INTRODUCTION

Recognition and removal of toxic and radioactive waste from water is of immense interest to national security, countering terrorism, and environmental protection.[1,2] Technetium is an important by-product of the nuclear industry, especially in nuclear reactors during the nuclear fission of uranium.[3,4] ^{99}Tc shows a long half-life ($t_{1/2} = 2.13 \times 10^5$ years) and exists primarily in its most stable oxidation state (VII), as pertechnetate ($^{99}TcO_4^-$). It is a huge challenge to remediate $^{99}TcO_4^-$ contaminated environment, for its high solubility in water and high environmental mobility.[5] Furthermore, direct study of TcO_4^- is extremely limited, considering its radioactivity and government restriction. As a result, its non-radioactive surrogate perrhenate (ReO_4^-) is usually used instead, which has similar charge density and thermodynamic parameters to TcO_4^-.

Due to the large size and low charge density, selective recognition and removal of TcO_4^- /ReO_4^- ions pose huge difficulty, especially after an accidental release of these anions into ground water. To date, several materials have been applied to immobilize or remove TcO_4^- ion from water, including anion-exchange resins,[6,7] supramolecular receptors,[8,9] crystalline inorganic cationic materials,[10] organic polymeric networks,[11–16] and coordination polymers (CPs).[17–20] Very recently, CPs showing the structural designability and diversity as well as outstanding functionalization, have been considered as promising candidates for selective anion receptors.[21–26]

As for selective recognition or detection, the current common instrumental methods, such as ion chromatography, inductively coupled plasma mass spectrometry (ICP-MS), and high-performance liquid chromatography coupled with atomic absorption spectrometry,

are expensive and time-consuming. In comparison, chemical luminescent sensors are more economical and convenient for detection. As a general strategy to TcO_4^-/ReO_4^- detection, a designed sensor with particular fluorophore interacting with the sorbed anions, will show significant changes of fluorescence.[27–29] In this way, the recognition and quantification of TcO_4^-/ReO_4^- can be achieved. Amendola et al have reported the first molecular receptor for $^{99}TcO_4^-$, which shows good turn off effect of the receptor's emission.[30] However, the capture ability was not mentioned and only the selectivity to monovalent anions (e.g. ClO_4^-, NO_3^-, and HSO_4^-) was demonstrated. Desai and Singh have reported a fluorescence turn on ReO_4^- sensor, Thioflavin-T, which shows ordinary selectivity (10-fold to competing anions) and detection limit (260 μM).[31] To our best knowledge, there is only one report on CP luminescent sensor for TcO_4^-/ReO_4^-.[32] Thereinto, MOR-1 and MOR-2 exhibit 62% and 63% emission quenching as determined by fluorescence titration. The whole process could be traced by fluorescence spectrometer. However, it cannot fulfill the requirements of field operation. In practice, the test paper strip is one of the fastest and easiest tools to detect the target species. Thus, a real-time test paper strip for sensing TcO_4^-/ReO_4^- is of great interest and necessity.

With this in mind, we have designed and prepared a unique CP-based test paper for ReO_4^- capture and detection. This CP is designated as TJNU-302 (TJNU denotes Tianjin Normal University), showing a 2-fold interpenetrated 3D cationic framework with the inclusion of lattice SbF_6^- anions. This material possesses fast exchange kinetics, high sorption capacity and distribution coefficient (K_d), and outstanding selectivity to ReO_4^- over other competing anions (500 times excess of CO_3^{2-} or PO_4^{3-}). As far as we know, TJNU-302 has the highest

quenching efficiency (86%) among all reported perrhenate sensors.[32] Owing to the fact that the TJNU-302 crystals can show an obvious quenching effect to perrhenate solution, a real-time test paper for ReO_4^- was fabricated. Moreover, the mechanism of ReO_4^- trapping by TJNU-302 has been revealed via single crystal to single crystal (SC-SC) transformation and further, supported by density functional theory (DFT) calculations.

EXPERIMENTAL SECTION

Materials and Methods. All chemicals were used as received without further purification. Here, the deionised water was used throughout. 1,2,4,5-Tetra(pyridin-4-yl)benzene (98%) was purchased from Tianjin Dadikanghe Co., Ltd. $KReO_4$ (99%) and $AgSbF_6$ (>98%) were purchased from Tianjin Chemical Technology Co., Ltd. The nylon membrane filter (0.22 μm) was purchased from Tianjin Navigator Lab Instrument Co., Ltd, which shows a small ReO_4^- sorption capacity of only 3.90% toward the $KReO_4$ water solution (500 ppm), as determined by ICP-OES. Elemental analysis was performed on a Vario EL III elemental analyzer. FT-IR spectra (KBr pellet) were taken on a Bruker Alfa FT-IR spectrometer. Powder X-ray diffraction (PXRD) patterns were recorded on a Rigaku model Ultima IV diffractometer with Rigaku D/teX ultrahigh-speed position sensitive detector and Cu-Kα X-ray (40 kV and 100 mA), by using a step-scan mode with a scan rate of 2 °/min and step size of 0.02°. Simulation of PXRD patterns was taken using the diffraction-crystal module of *Mercury* based on single-crystal diffraction data. Scanning electron microscopy (SEM) and energy-dispersive X-ray spectroscopy (EDS) were conducted on a FEI Nova Nano 230 scanning electron microscope with the electron beam energy of 15 or 20 keV. Inductively

coupled plasma mass spectroscopy (ICP-MS) analysis was performed with a Perkin-Elmer ELAN 9000 instrument after digestion of the sample in HNO_3. Inductively coupled plasma optical emission spectrometer (ICP-OES) analysis was taken using a Perkin-Elmer Avio 200 instrument after digestion of the sample in HNO_3. Fluorescence spectra were recorded on a FL-1065 spectrometer.

Single-Crystal X-Ray Diffraction. Single crystal X-ray diffraction (SC-XRD) data were collected on an Agilent SuperNova Dual diffractometer with an AtlasS2 detector and Cu Kα radiation (λ = 1.54184 Å) at 293 K for both TJNU-302 and TJNU-302(Re). Multi-scan absorption corrections were performed using the SADABS program. The structures were solved by direct methods, and all non-hydrogen atoms were refined anisotropically by full-matrix least-squares method with *SHELXTL* software package. The final refinements were conducted by full-matrix least-squares methods with anisotropic thermal parameters for all non-H atoms on F^2. Generally, C-bound H atoms were geometrically located and refined using the riding model. Isotropic displacement parameters of H atoms were derived from their parent atoms. Further crystal data and structural refinement details are listed in Table S1 and selected bond lengths and angles are shown in Table S2 (Supporting Information).

Synthesis of [Ag(1,2,4,5-p4b)](SbF$_6$) (TJNU-302). A CH_3OH solution (3 mL) of 1,2,4,5-p4b (19.3 mg, 0.05 mmol) was carefully layered on an aqueous solution (3 mL) of $AgSbF_6$ (17.1 mg, 0.05 mmol), with ethyl acetate as the intermediate layer in a straight glass tube. Colorless block crystals were obtained by slow evaporation of solvent at room temperature after three days. Yield: ca. 32 mg. Anal. calcd for $C_{26}H_{18}N_4F_6SbAg$: C, 42.77; H, 2.49; N,

7.67%. Found: C, 42.57; H, 2.44; N, 7.72%. FT-IR (cm^{-1}): 1603*vs*, 1547*m*, 1475*w*, 1420*s*, 1219*m,* 1068*m*, 1011*m*, 825*s*, 747*w*, 630*vs*, 562*m*, 541*m.*

Synthesis of [Ag(1,2,4,5-p4b)](ReO$_4$) (TJNU-302(Re)). As-preapred TJNU-302 crystals (15 mg) were immersed in an aqueous solution of $KReO_4$ (5 mL, 0.05 mmol) for one day. Good quality crystals were isolated. Anal. calcd for $C_{26}H_{18}AgN_4O_4Re$: C, 41.94; H, 2.44; N, 7.53%. Found: C, 41.95; H, 2.43; N, 7.52%. FT-IR (cm^{-1}): 1593*vs*, 1543*m*, 1473*w*, 1407*s*, 1213*w,* 1090*w*, 1051*s*, 993*vs*, 912*vs*, 818*s*, 557*m*.

Typical Perrhenate Adsorption Method. As-synthesized TJNU-302 crystals (37 mg, ca. 0.05 mmol) were added to a water solution (20 mL) of $KReO_4$ (58 mg, 0.2 mmol) and the mixture was stirred at room temperature. The solids were monitored using FT-IR, PXRD, SEM-EDS elemental mapping and ICP-OES at various time intervals.

Adsorption Data Fitting by Kinetics Model. As-synthesized TJNU-302 crystals (110 mg, ca. 0.15 mmol) were immersed into an aqueous solution (30 mL) of $KReO_4$ (0.03 mmol) and stirred at room temperature. Then, the solution was separated at different time intervals by a nylon membrane filter (0.22 μm). The concentration of ReO_4^- remaining in the water phase and the corresponding ReO_4^- removal percentage by TJNU-302 were determined by ICP-OES measurement. The equation of linearized form of pseudo-second-order model is shown in equation (1), where the measured q_t and q_e (mg g^{-1}) are the ReO_4^- uptake amount at t min and at equilibrium, respectively, and k_2 (g mg^{-1} min^{-1}) is the pseudo-second-order rate constant.

$$\frac{t}{q_t} = \frac{t}{q_e} + \frac{1}{k_2 q_e^2} \qquad (1)$$

Adsorption Data Fitting by Isotherm Models. As-synthesized TJNU-302 crystals (5 mg) were immersed into an aqueous solution (10 mL) of $KReO_4$ with the concentration of 500, 450, 400, 300, 250, 150, 100, 25, or 20 ppm. The mixture was stirred at room temperature for 24 h to make sure that an equilibrium was achieved, after which the concentration of residual ReO_4^- ion in water phase was unchanged as determined by ICP-MS. The solution was separated from the crystals with a nylon membrane filter (0.22 μm). The concentration of residual ReO_4^- in water phase and the trapping percentage of ReO_4^- were measured by ICP-MS. In order to determine the adsorption thermodynamics of ReO_4^- by TJNU-302, Langmuir and Freundlich sorption models were used.

In the Langmuir model, the adsorption was assumed to occur on a homogeneous solid surface of TJNU-302, following a monolayer sorption process. The equation of Langmuir model is

$$\frac{c_e}{q_e} = \frac{1}{q_m k_L} + \frac{c_e}{q_m} \qquad (2)$$

where c_e is the equilibrium concentration of anions (mg L^{-1}), q_e and q_m are the equilibrium and maximum sorption amounts (mg g^{-1}), and k_L is a constant indirectly related to sorption amount and energy of sorption (L mg^{-1}). The fitting line was carried out by plotting c_e/q_e against c_e. The values of q_m and k_L can be calculated from the slope and intercept.

The Freundlich adsorption model is based on a heterogeneous surface, which suggests different binding energies between the anions and surface sites of TJNU-302. The equation of the Freundlich model is

$$\ln q_e = \ln k_F + \frac{1}{n} \ln c_e \qquad (3)$$

where c_e and q_e are the equilibrium concentration of anions (mg L^{-1}) and the equilibrium sorption amount (mg g^{-1}), and k_F and n are the Freundlich constants, which are related to sorption amount (mg g^{-1}) and adsorption intensity, characterizing the affinity of adsorbate with the adsorbent.

Hydrolytic Stability. As-synthesized TJNU-302 crystals (20 mg) were immersed in HNO_3 or NaOH solution of different pH values and stirred at room temperature for 24 h. Then, the solid was collected by filtration and washed with water several times. The solids were further used to remove 50 ppm ReO_4^- from the water solutions. The concentration of ReO_4^- ion remaining in the water phase and the corresponding trapping percentage of ReO_4^- were determined by ICP-MS. The solids were washed with water, dried, and characterized using PXRD.

Anion Selectivity. The competing effect with other anions, including SO_4^{2-}, CO_3^{2-}, NO_3^-, PO_4^{3-}, CF_3COO^-, $CH_3SO_3^-$, and F^-, was performed by adding TJNU-302 (10 mg) into an aqueous solution of ReO_4^- (10 mL, 0.025 mmol L^{-1}) containing another type of anion (in mmol L^{-1}), e.g. 25 Na_2SO_4, 2.5 Na_2CO_3, 1.25 $NaNO_3$, 1.25 K_3PO_4, 0.5 CF_3COONa, 0.5 CH_3SO_3Na, or 0.25 NaF. Then, the sample was washed with water, dried and characterized using FT-IR. Further, the effect of CO_3^{2-} (or PO_4^{3-}) was tested by adding 10 mg of TJNU-302 to the ReO_4^- solution (10 mL, 0.025 mmol L^{-1}) containing 2.5, 5.0, 7.5, 10.0 and 12.5 mmol L^{-1} Na_2CO_3 (or K_3PO_4), respectively. The concentration of ReO_4^- ion in water after adsorption was determined by ICP-MS.

Recyclability

In the first cycle, TJNU-302 (50 mg) was immersed in a $KReO_4$ solution (20 mL, 180 ppm) for 24 h. After that, the ReO_4^- sorbed material was stirred in $NaSbF_6$ solution (1 mol L^{-1}, 50 mL) under heating at 50 °C. The solid was collected by centrifugation. Such recovered material was then subject to the next recyclability. Stability of regenerated TJNU-302 was verified by PXRD and the ReO_4^- removal ratio in each run was determined by ICP-OES.

Preparation of TJNU-302 Suspension for Luminescent Sensing. A water suspension of TJNU-302 was prepared by dispersing 1 mg TJNU-302 crystals into 3 mL water, followed by the ultrasonic treatment for 20 min, and then used in the following tests.

Fluorescence Response to ReO_4^-. Titration experiment for sensing $KReO_4$ was performed by a continuous addition of $KReO_4$ solution (0.02 mol L^{-1}) into the TJNU-302 suspension. The quenching percentage (QP) was calculated with $(1 - I/I_o) \times 100\%$ and the quenching effect of $KReO_4$ was quantified by Stern-Volmer constant (K_{sv}), which was calculated from the Stern-Volmer equation $I_0/I = K_{sv}[M] + 1$. Herein, I_0 and I are the luminescence intensity without and with adding $KReO_4$ solution, respectively, and [M] is the molar concentration of quencher ReO_4^-.

Effect of pH on Fluorescence Response to ReO_4^-. The TJNU-302 suspensions (3 mL) at different pH values (e.g. 3, 5, 7, 10, and 13) were prepared by mixing with HNO_3 or NaOH solution. After that, $KReO_4$ solution (200 μL, 0.02 mol L^{-1}) was added to each suspension. The luminescence intensity of each sample was collected.

Fluorescence Response to Other Anions. An aqueous solution of SO_4^{2-} (100 μL, 0.2 mol L^{-1}) was added into TJNU-302 suspension. After ca. 5 min, the luminescence of suspension

was measured and the quenching percentage was calculated by equation $(1 - I/I_o) \times 100\%$. The fluorescence responses to CO_3^{2-}, Cl^-, NO_2^-, and NO_3^- were similarly studied.

Fluorescence Response to Low Activity Waste (LAW). A simulated Hanford LAW Melter Recycle Stream was prepared, in which TcO_4^- was replaced with ReO_4^- (Table S3, Supporting Information).[11] In addition, a simulated LAW solution without ReO_4^- ion was prepared for comparison. Then, a 100 μL simulated LAW solution with or without ReO_4^- anion was added into the TJNU-302 suspension. After 5 min, the fluorescence intensity of suspension was tested and the quenching percentage was calculated by $(1 - I/I_o) \times 100\%$.

Computational Methods. All calculations were carried out with density functional theory (DFT) within the projected-augmented plane wave method[33,34] as implemented in Vienna ab initio simulation package (VASP).[35] The generalized gradient approximation suggested by Perdew, Burke, and Ernzerhof with London dispersion corrections proposed by Grimme (PBE-D2) was employed to accurately describe the weak interactions.[36,37] The Monkhorst-Pack mesh was employed to sample the Brillouin zone for geometry optimizations and electronic structure calculations.[38] In current calculations, a plane-wave cutoff energy of 500 eV was used and all atomic positions were relaxed at the PBE level until the atomic force was less than 0.01 eV $Å^{-1}$. The tolerance for energy convergence was set to 10^{-5} eV.

RESULTS AND DISCUSSION

Crystal Structure of TJNU-302. The targeted TJNU-302 material was designed based on Ag(I) cation and 1,2,4,5-p4b ligand, which bears four binding sites and may adopt diverse

conformations caused by the rotation of pyridyl groups. Such a flexible and neutral ligand will facilitate the construction of cationic coordination network with Ag(I) ions.

Structural analysis of TJNU-302 crystal reveals that it is monoclinic with a = 14.1795(3), b = 8.7989(2), c = 20.5217(4) Å, β = 102.312(2)°, and space group $P2_1/n$ (Table S1, Supporting Information). The asymmetric unit is composed by one Ag(I) center, two half 1,2,4,5-p4b ligands, and one SbF_6^- anion (Figure 1a). Each Ag(I) center is ligated by three 1,2,4,5-p4b ligands to constitute a trigonal geometry. For the two 1,2,4,5-p4b ligands, their coordination modes are different, where one (N1,N3) is a square-planar linker and the other (N2,N4) is a linear linker. As a consequence, the Ag(I) ions are linked by the 1,2,4,5-p4b ligands to form a 3D coordination network. Moreover, two such networks are intertangled to afford a 2-fold interpenetrating architecture, with the inclusion of SbF_6^- anions (Figure 1b). By considering each Ag(I) ion and each (N1,N3)-1,2,4,5-p4b ligand as the nodes, this 3D network can be simplified into a (3,4)-connected $(8^3)_2(8^5 10)$ topology prototype (Figure S1, Supporting Information).

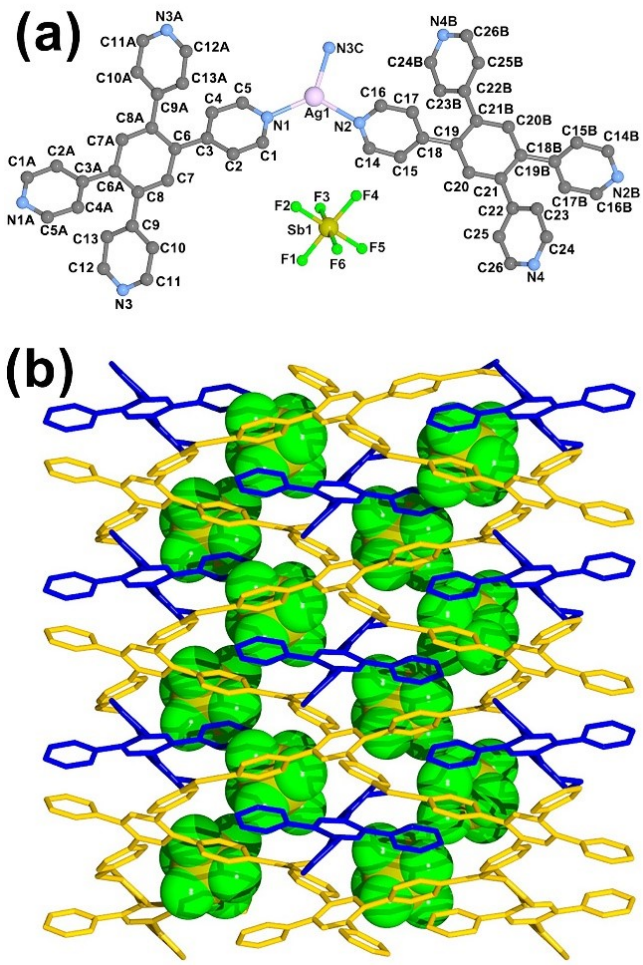

Figure 1. Crystal structure of TJNU-302. (a) Coordination environment of Ag(I) and location of SbF_6^- anion. (b) Two-fold interpenetrated architecture of TJNU-302, showing the included SbF_6^- anions in space-filling model.

ReO_4^- Sorption. Anion exchange of ReO_4^- was explored by immersing TJNU-302 crystals (37 mg, ca. 0.05 mmol) into an aqueous solution (20 mL) of $KReO_4$ (58 mg, ca. 0.2 mmol). The process was monitored by FT-IR, PXRD, SEM-EDS elemental mapping and ICP-OES. As shown in Figure 2a, a new strong IR peak appears at ca. 902 cm^{-1} within 1 min of anion exchange, revealing the formation of ReO_4^--loaded TJNU-302. When the anion-exchange proceeds for 10 min, the intensity of IR peak at 902 cm^{-1} further increases, but the peak at 631 cm^{-1} of SbF_6^- disappears, indicating the completion of anion exchange.

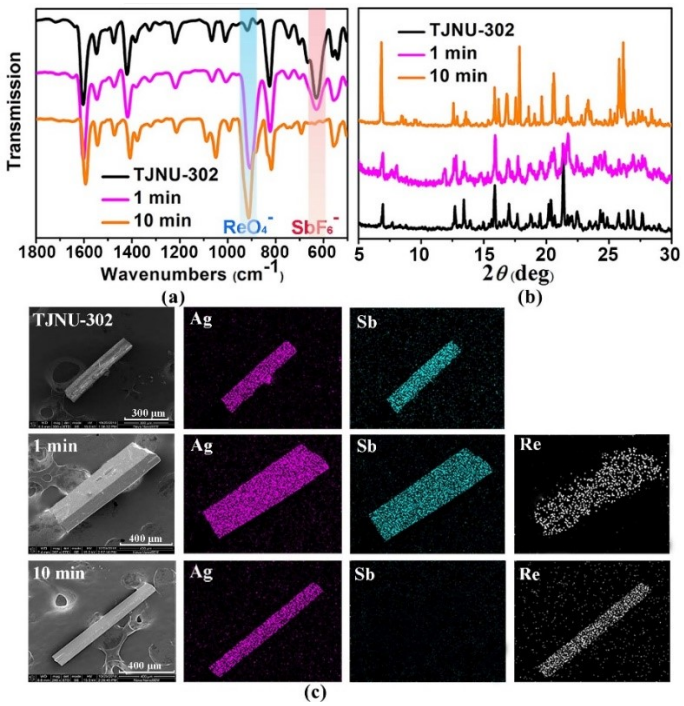

Figure 2. (a) FT-IR spectra and (b) PXRD patterns of TJNU-302 at different anion-exchange levels. (c) The corresponding SEM images and EDS elemental mappings of Ag, Sb and Re for the crystals.

The PXRD patterns of both the initial and final samples show good crystallinity, whereas the sample after 1 min of anion-exchange shows a relatively low crystallinity (Figure 2b). Nevertheless, the crystal morphology is well retained after the reaction. Figure 2c shows the SEM images of typical crystals from the samples, together with their elemental maps of Ag, Sb, and Re. Clearly, Ag is from the TJNU-302 framework and its distribution does not change during the anion-exchange. Other than Ag, the original TJNU-302 crystal only contains Sb, while the crystal after anion-change for 10 min shows only Re. As anticipated, the crystal after 1 min of anion-exchange contains evenly distributed Sb and Re. The final product was also characterized by ICP-OES, which reveals that all SbF_6^- in TJNU-302 can be quantitatively exchanged by ReO_4^-.

To further evaluate the ability of TJNU-302 as scavenger for ReO_4^- removal, the sorption kinetics was studied by soaking TJNU-302 crystals (110 mg, ca. 0.15 mmol) into a $KReO_4$ solution (0.03 mmol, 30 mL). As determined by ICP-OES analysis of the solution, 97.1% and 99.9% of ReO_4^- anions were rapidly removed after 5 and 10 min, respectively (Figure 3a). The kinetics for ReO_4^- sorption from water can be described by Equation (1) given in the Experimental Section. As a result, it shows a pseudo-second-order reaction with a very good correlation coefficient (0.999), and the pseudo-second-order rate constant k_2 (0.1022 g mg^{-1} min^{-1}) can be obtained from the fitted plots via t/q_t vs. t.

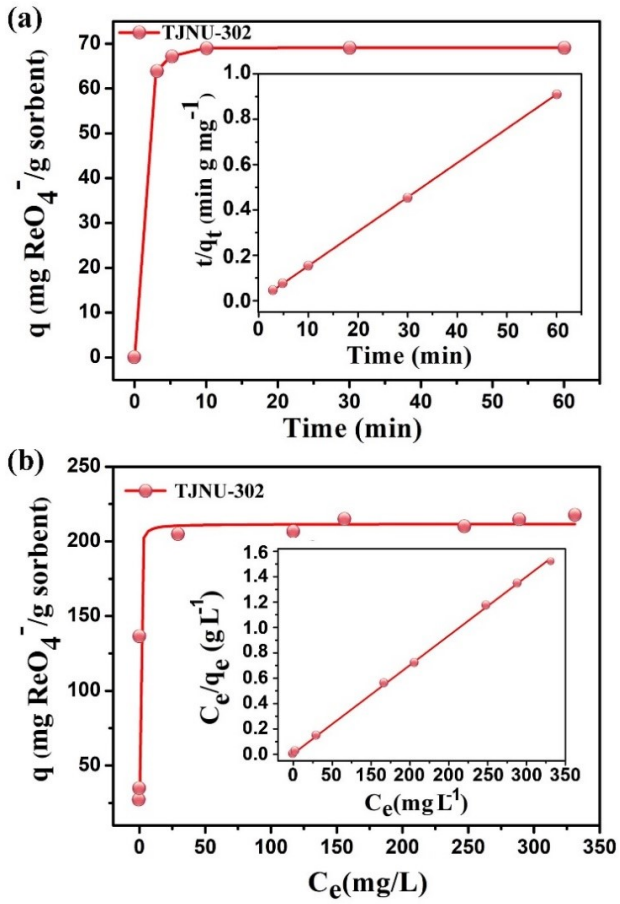

Figure 3. (a) ReO_4^- sorption curve vs. time in TJNU-302 suspension. Inset: Pseudo-second-order kinetic plot for sorption. (b) ReO_4^- sorption curve vs. concentration in TJNU-302 suspension. Inset: Fitting the equilibrium sorption data with Langmuir model.

To further explore the adsorption thermodynamic properties for ReO_4^-, 5 mg TJNU-302 were immersed in a 10 mL water solution with different concentrations of $KReO_4$ (20−500 ppm). Langmuir and Freundlich sorption models were applied. As a result, the adsorption isotherm of TJNU-302 can be fitted with Langmuir model (Figure 3b).[39] The correlation coefficient is high (> 0.99) and the calculated maximum adsorption capacity for ReO_4^- is 211 mg per gram of TJNU-302. In addition, the exact amount of Re(VII) adsorption (256 mg per gram) was calculated using the crystal structure data, which is slightly higher but can be experimentally achieved by using a saturated ReO_4^- water solution. Moreover, the distribution coefficient (K_d) is usually used to evaluate the performance of anion scavenger, and a K_d value above 1.0×10^5 mL g^{-1} is considered to be excellent.[40] The K_d value can be calculated by using the equation $K_d = [(C_0 - C_e)V/C_e]/m$, in which C_0 and C_e are the initial and equilibrium concentrations of ReO_4^- (mL g^{-1}), V is the volume of the treated solution (mL), m is the mass of TJNU-302 (g). Herein, the K_d value of TJNU-302 for ReO_4^- was calculated to be 5.8×10^5 mL g^{-1}, which is one of the highest for TcO_4^-/ReO_4^- adsorption materials reported so far (Table S4, Supporting Information).[41]

Hydrolytic Stability, Recyclability and Anion Selectivity. The hydrolytic stability under different pH conditions and recyclability are both critical to anion-exchange materials in practical applications. As demonstrated by PXRD patterns (Figure 4a), TJNU-302 is stable over a wide pH range from 3 to 13. However, TJNU-302 will be dissolved in an aqueous solution of pH = 2 and be decomposed (Figure S2, Supporting Information) in an aqueous solution of pH = 14. Significantly, the ReO_4^- removal percentages in the pH range of 6–9 are nearly 100% (Figure 4b). Moreover, a slight mass loss of only 6.2% and 5.6% is found

for TJNU-302 solid before and after the treatment by water solutions with pH = 3 and 13, respectively, further indicating its hydrolytic stability.[42] Additionally, the ReO_4^--loaded TJNU-302 can be regenerated by washing with $NaSbF_6$ solution at least for six cycles, as revealed by PXRD patterns (Figure S3, Supporting Information). The regenerated TJNU-302 can also remove ca. 82% ReO_4^- from the water solution (Figure 4c). This is significant for such a porous sorbent, since the cost of TJNU-302 is ca. 500 US dollars per kilogram.

Most TcO_4^-/ReO_4^- sorbents, especially inorganic cationic materials and anion-exchange resins, normally exhibit low selectivity in the presence of competing anions (e.g. carbonate and phosphate).[6–9] To this end, the competing selectivity for CO_3^{2-}/ReO_4^- and PO_4^{3-}/ReO_4^- was explored. As shown in Figure 4d, the removal percentages of ReO_4^- remain as high as 83.2% and 81.7% for TJNU-302, even the concentration of CO_3^{2-} and PO_4^{3-} is 500 times in excess. Further, the removal percentages of ReO_4^- by TJNU-302 are all as high as over 80%, in the presence of 1000 times of SO_4^{2-}, 50 times of NO_3^-, 20 times of CF_3COO^-, 20 times of $CH_3SO_3^-$, and 10 times of F^- in excess (Figure S4, Supporting Information).

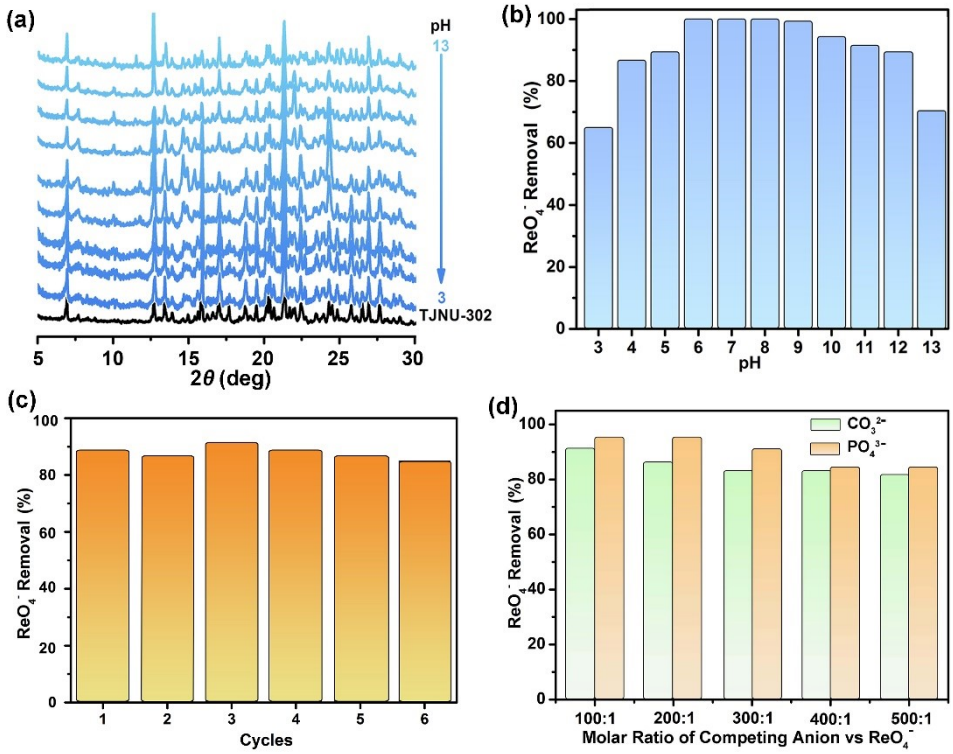

Figure 4. (a) PXRD patterns of TJNU-302 after soaking in water solutions with pH = 3–13. (b) Removal percentages of ReO_4^- by TJNU-302 under pH = 3–13. (c) Removal percentages of ReO_4^- by TJNU-302 after different cycles. (d) Removal percentages of ReO_4^- by TJNU-302 in ReO_4^-/CO_3^{2-} or ReO_4^-/PO_4^{3-} mixtures with various ratios.

Structure-Property Correlation. The underlying reason for outstanding ReO_4^- removal selectivity by TJNU-302 can be elucidated based on a molecular-scale analysis. Recently, SC-SC transformation has been considered as the most convincing approach to study anion exchange process, with the aid of single crystal X-ray diffraction technique.[43] Herein, the ReO_4^--loaded crystal TJNU-302(Re), namely [Ag(1,2,4,5-p4b)](ReO_4), was successfully obtained. TJNU-302(Re) is monoclinic with a = 14.3428(3), b = 8.6193(2), c = 20.2530(5) Å, β = 101.798(2)°, and space group $P2_1/n$. It can be viewed as an isostructure of TJNU-302, with changes of the unit cell parameters of +1.2%a, –2.0%b, –1.3%c, –0.51°β and –

2.0%V (Table S1, Supporting Information). Structural analysis shows that each ReO_4^- ion can be firmly trapped by four hydrogen bonds with pyridyl groups of 1,2,4,5-p4b, with the H···O distances in 2.55–2.59 Å range (Figure 5 and Table S5, Supporting Information). Moreover, SiF_6^{2-} anion has a radius of 2.59 Å, which is very similar to that of ReO_4^- (2.60 Å).[44] These structural features are beneficial to provide matching space for ReO_4^- trapping.

As stated above, TJNU-302 has a high sorption selectivity to ReO_4^-, which is attributed to a combination of favorable charge and size of ReO_4^- ion for the host-guest interaction. ReO_4^- is a monovalent anion with large size, overall showing a lower charge density. Thus, compared to SO_4^{2-}, CO_3^{2-}, NO_3^-, PO_4^{3-}, CF_3COO^-, $CH_3SO_3^-$, and F^-, ReO_4^- anion is more hydrophobic and readily to transport from the water solution to anion-exchange materials. According to the experiments and Mulliken population analysis, both TcO_4^-/ReO_4^- anions have low hydration energy and only modest charge density on oxygen atoms.[44] In detail, the hydration energy ($\Delta G_h°$) is significantly different between ReO_4^- (–330 kJ mol^{-1}) and CO_3^{2-} (–1315 kJ mol^{-1}) / PO_4^{3-} (–2773 kJ mol^{-1}).[5,45] That is, it is unnecessary for ReO_4^- to overcome a high energy barrier during dehydration. Due to the hydrophobicity of the pores for TJNU-302, it prefers trapping ReO_4^- than CO_3^{2-} and PO_4^{3-}. In addition, the presence of multiple hydrogen-bonding interactions will also boost its anion-exchange selectivity.

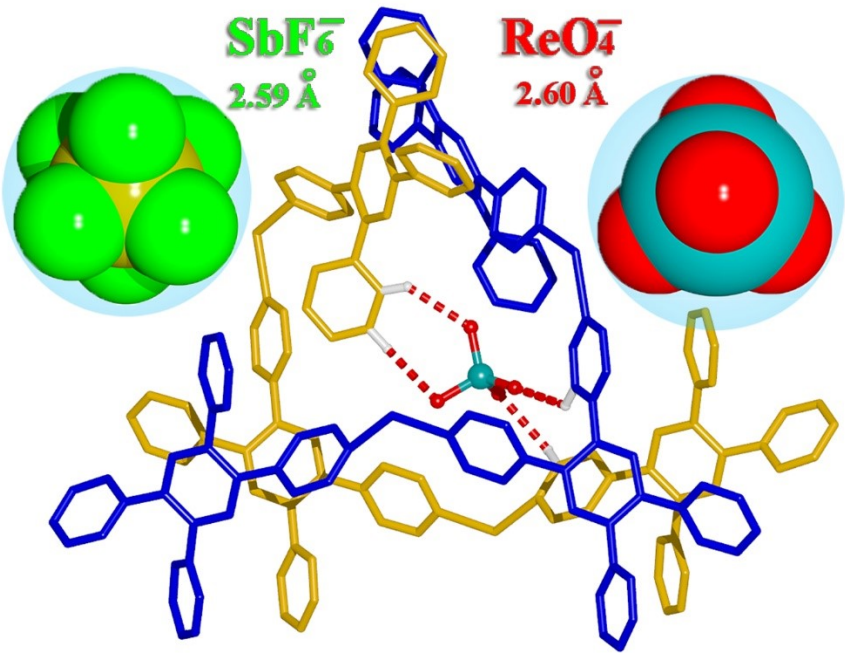

Figure 5. Schematic drawing of the anion radii for SbF_6^- and ReO_4^-, and multiple hydrogen bonds between ReO_4^- and the coordination network in TJNU-302(Re).

To further illustrate the intrinsic driving force for ReO_4^- trapping by TJNU-302, the DFT calculations were performed for TJNU-302 and TJNU-302(Re). Molecular orbital analyses indicate that there is scarcely any interaction between the *p* orbitals of F in SbF_6^- and the π orbitals of imidazole ring in TJNU-302 (Figure S5, Supporting Information). However, in TJNU-302(Re), the π bonds hybridize with the *p* lone pair electrons of ReO_4^- anions, which indicate the relatively strong interactions.

Luminescence Sensing. The luminescent properties of TJNU-302 in water solution were initially investigated with a handheld UV lamp. Upon 254 nm irradiation, a noticeable and typical fluorescence of the TJNU-302 crystals appears (Figure 6a left). While in the ReO_4^- solution, a fluorescent quenching effect is observed for the crystals (Figure 6a right). This is a solid-state luminescence sensor for ReO_4^- anion, which is clearly more convenient than

the reported suspension sensors. To further evaluate its practicability, a test paper for ReO_4^- was fabricated. In detail, a piece of filter paper was dipped into a water solution (3 mL) of TJNU-302 (1 mg), and then allowed to air-dry. By using an ink of ReO_4^- (0.02 mol L^{-1}), a written word of "Re" clearly appears on the test paper under 254 nm irradiation (Figure 6b inset).

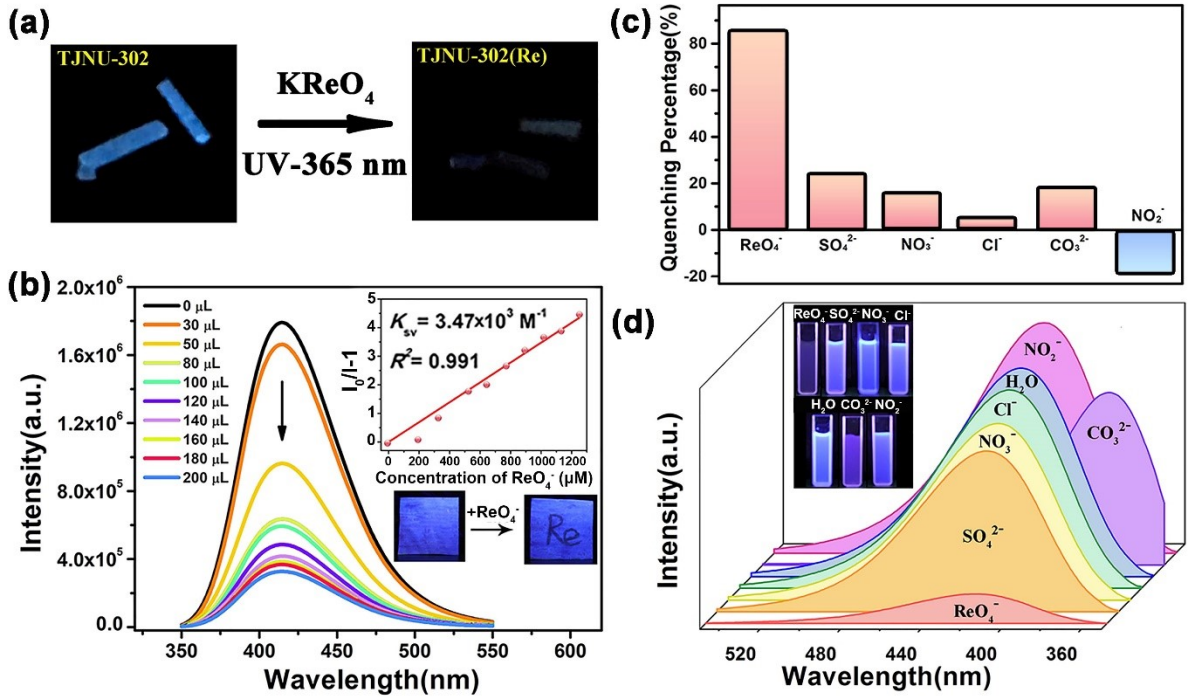

Figure 6. (a) UV photos of TJNU-302 crystals before and after immersing in $KReO_4$ water solution. (b) The emission spectra and K_{sv} value of TJNU-302 titrated with $KReO_4$ water solution. Inset: the photos of test paper experiment for ReO_4^-. (c) Luminescence quenching percentages and (d) emission spectra of TJNU-302 in water solutions containing different anions. Inset: corresponding luminescence photos of TJNU-302.

To further determine the sensing performance of TJNU-302, the fluorescence quenching experiments were performed through stepwise adding the water solution (0.02 mol L^{-1}) of

$KReO_4$. As shown in Figure 6b, the aqueous suspension of TJNU-302 exhibits an obvious emission at 416 nm upon exciting at 324 nm. In comparison, a similar emission is found at 373 nm (Figure S6, Supporting Information) for the 1,2,4,5-p4b ligand, upon exciting at 300 nm. Therefore, the origin of fluorescence emission for TJNU-302 could preliminarily be attributed to ligand-centered π–π* transitions and/or the incorporation of metal–ligand interactions.[46] By adding $KReO_4$ water solution, the emission intensity decreases with the quenching percentage (QP) of 86% at most for TJNU-302 suspension. Based on the Stern-Volmer equation, a good linear relationship with the correlation coefficient (R^2) of 0.991 and quenching constant (K_{sv}) of 3.47×10^3 L mol^{-1} can be obtained. The limit of detection (LOD) is 90 μM, as calculated according to 3σ/slope. Here, σ is determined by the equation $\sigma = 100 \times (I_{SE}/I_0)$, in which I_{SE} is the standard error of the blank measurement and I_0 is the measured luminescence intensity of TJNU-302 in water. Although several materials show the turn-on or turn-off luminescent sensing to ReO_4^-/TcO_4^- ions, TJNU-302 significantly has the highest quenching efficiency (Table S6, Supporting Information). To illustrate the effect of pH on the sensing performances, $KReO_4$ water solution was added to the aqueous suspensions of TJNU-302 of different pH values. Similar quenching were also observed (Figure S7, Supporting Information) to reveal the pH-independent sensing performance.

The outstanding sensing ability of TJNU-302 toward ReO_4^- promotes us to further study its response to other anions in the simulated Hanford LAW Melter recycle stream. A finely ground powder of TJNU-302 (1 mg) was dispersed into 3 mL water solution, to which 100 μL of 0.2 mol L^{-1} anion solution (SO_4^{2-}, NO_3^-, Cl^-, CO_3^{2-} or NO_2^-) or 100 μL of 0.02 mol L^{-1} ReO_4^- solution was added. As shown in Figures 6c and 6d, although the molar ratio of

anion: ReO_4^- is 10: 1, TJNU-302 exhibits the highest quenching percentage toward ReO_4^-. For Cl^-, NO_3^-, CO_3^{2-}, and SO_4^{2-} anions, it shows the quenching percentages of 4.6–27.7%. However, the addition of CO_3^{2-} to TJNU-302 suspension leads to the shift of fluorescence emission to 377 nm. A possible explanation is that the CO_3^{2-} anion could strongly interact with Ag(I) center to break the charge transfer between metal and ligand.[47,48] Therefore, the fluorescence emission is likely to derive from ligand-centered π–π* transitions (Figure S6, Supporting Information).[49] As for NO_2^- ion, the luminescence intensity slightly increases by 10.5%. We may conclude that, the incorporated nitrite acts as electron donating moiety to generate hydrogen-bonding interaction with the ligand, promoting the electron transfer between metal and ligand.[30,50] Moreover, by adding the simulated Hanford LAW Melter Recycle stream (100 μL) to TJNU-302 (1 mg) suspension, the luminescence intensity will increase by 14.6% (Figure S8, Supporting Information). This is due to the high molar ratio of NO_2^-: ReO_4^- (873: 1). In contrast, when the simulated stream of LAW without ReO_4^- was added to the suspension of TJNU-302, the fluorescence intensity largely increased by 46.9%, revealing the quenching effect of ReO_4^-.

It is critical to study the luminescence mechanism of TJNU-302 in order to elucidate its luminescent quenching to ReO_4^-/TcO_4^-. As stated above, the π-conjugated aromatic ligand in TJNU-302 plays an essential role in its fluorescence properties (Figure S6, Supporting Information).[51] Generally, two possible mechanisms may be hypothesized for such sensing systems. First, the UV-vis absorption peaks of TJNU-302 and ReO_4^- show a partial overlap (Figure S9, Supporting Information). Thus, the competition of ReO_4^- and host framework in absorbing the excitation light may lead to the luminescent quenching.[52–54] Moreover, the

intramolecular deactivation must be taken into account. Since TJNU-302 is stable in water solution of ReO_4^-, the quenching is not a result of degradation of the crystalline phase and instead, of the interaction between the chromophore (ligand) and ReO_4^-. As confirmed by SC-XRD, ReO_4^- could establish strong H-bonding interactions with the host framework. As a result, H-bonding interactions between the anion and host framework may destabilize the orbital energy level of sp^2 C, which promote the intramolecular electron transformation. Thus, it can be concluded that the ligand-to-ReO_4^- electron transfer will also be responsible for the observed fluorescence quenching.[30,32,55]

CONCLUSION

In this work, a cationic CP sensor has been designed and synthesized for detection of ReO_4^- anion, which shows the highest efficiency among all reported ReO_4^- sensors. This porous material also exhibits high ReO_4^--exchange capacity and selectivity, which can be properly explained by the molecular-scale crystal structure analysis of the anion-exchange product via SC-SC transformation, and further verified by DFT calculations. Remarkably, relying on the solid-state UV-quenching effect of TJNU-302 on perrhenate, a ReO_4^- test paper can be produced. The results will not only present a new CP material with potential application in design of instant sensors, but also provide useful insights into understanding the anion-exchange process or mechanism for such porous crystalline materials.

ASSOCIATED CONTENT

Supporting Information. The Supporting Information is available free of charge on the ACS Publications website at DOI: 10.1021/acsami.xxxxxxx.

Tables for Crystallographic parameters, selective bond lengths and angles, composition of simulated Hanford LAW melter off-gas scrubber solution, adsorption efficiency of ReO_4^-, hydrogen-bonding geometries, comparison of the reported luminescent sensors; Figures for topological network of TJNU-302, PXRD patterns under different conditions, FT-IR and removal percentages of ReO_4^- and competing anions, molecular orbital interaction, and luminescent and UV-vis spectra.

AUTHOR INFORMATION

Corresponding Author

E-mail: hxxydm@tjnu.edu.cn (M. Du), wzhou@st-andrews.ac.uk (W. Zhou)

Notes

The authors declare no competing financial interest.

ACKNOWLEDGMENTS

This work was financially supported by the National Natural Science Foundation of China (21771139), Tianjin Natural Science Foundation (17JCYBJC22800), and the Program for Innovative Research Team in University of Tianjin (TD13-5074).

REFERENCES

[1] Oliver, S. R. J. Cationic Inorganic Materials for Anionic Pollutant Trapping and Catalysis. *Chem. Soc. Rev.* **2009**, *38*, 1868-1881.

[2] Smith, F. N.; Taylor, C. D.; Um, W.; Kruger, A. A. Technetium Incorporation into Goethite (α-FeOOH): An Atomic-Scale Investigation. *Environ. Sci. Technol.* **2015**, *49*, 13699-13707.

[3] Lumetta, G. J.; Moyer, B. A.; Singh, R. P. *Fundamentals and Applications of Anion Separations*; Kluwer Academic / Plenum: New York, USA, 2004.

[4] Attix, F. H. *Introduction to Radiological Physics and Radiation Dosimetry*; Wiley-VCH: Weinheim, Germany, 1986.

[5] Banerjee, D.; Kim, D.; Schweiger, M. J.; Kruger, A. A.; Thallapally, P. K. Removal of TcO_4^- Ions from Solution: Materials and Future Outlook. *Chem. Soc. Rev.* **2016**, *45*, 2724-2739.

[6] Li, J.; Zhu, L.; Xiao, C.; Chen, L.; Chai, Z.; Wang, S. Efficient Uptake of Perrhenate/Pertechnetate from Aqueous Solutions by the Bifunctional Anion-Exchange Resin. *Radiochim. Acta* **2018**, *106*, 581-591.

[7] Bonnesen, P. V.; Brown, G. M.; Alexandratos, S. D.; Bavoux, L. B.; Presley, D. J.; Patel, V.; Ober, R.; Moyer, B. A. Development of Bifunctional Anion-Exchange Resins with Improved Selectivity and Sorptive Kinetics for Pertechnetate: Batch-Equilibrium Experiments. *Environ. Sci. Technol.* **2000**, *34*, 3761-3766.

[8] Katayev, E. A.; Kolesnikov, G. V.; Sessler, J. L. Molecular Recognition of Pertechnetate and Perrhenate. *Chem. Soc. Rev.* **2009**, *38*, 1572-1586.

[9] Lim, J. Y. C.; Beer, P. D. Superior Perrhenate Anion Recognition in Water by a Halogen Bonding Acyclic Receptor. *Chem. Commun.* **2015**, *51*, 3686-3688.

[10] Wang, S.; Yu, P.; Purse, B. A.; Orta, M. J.; Diwu, J.; Casey, W. H.; Phillips, B. L.; Alekseev, E. V.; Depmeier, W.; Hobbs, D. T.; Albrecht-Schmitt, T. E. Selectivity, Kinetics, and Efficiency of Reversible Anion Exchange with TcO_4^- in a Supertetrahedral Cationic Framework. *Adv. Funct. Mater.* **2012**, *22*, 2241-2250.

[11] Sun, Q.; Zhu, L.; Aguila, B.; Thallapally, P. K.; Xu, C.; Chen, J.; Wang, S.; Rogers, D.; Ma, S. Optimizing Radionuclide Sequestration in Anion Nanotraps with Record Pertechnetate Sorption. *Nat. Commun.* **2019**, *10*, 1646.

[12] Banerjee, D.; Elsaidi, S. K.; Aguila, B.; Li, B.; Kim, D.; Schweiger, M. J.; Kruger, A. A.; Doonan, C. J.; Ma, S.; Thallapally, P. K. Removal of Pertechnetate-Related Oxyanions from Solution Using Functionalized Hierarchical Porous Frameworks. *Chem. Eur. J.* **2016**, *22*, 17581-17584.

[13] Zhang, W.; Aguila, B.; Ma, S. Potential Applications of Functional Porous Organic Polymer Materials, *J. Mater. Chem. A* **2017**, *5*, 8795-8824.

[14] Li, J.; Dai, X.; Zhu, L.; Xu, C.; Zhang, D.; Silver, M. A.; Li, P.; Chen, L.; Li, Y.; Zuo, D.; Zhang, H.; Xiao, C.; Chen, J.; Diwu, J.; Farha, O. K.; Albrecht-Schmitt, T. E.; Chai, Z.; Wang, S. $^{99}TcO_4^-$ Remediation by a Cationic Polymeric Network. *Nat. Commun.* **2018**, *9*, 3007.

[15] He, L.; Liu, S.; Chen, L.; Dai, X.; Li, J.; Zhang, M.; Ma, F.; Zhang, C.; Yang, Z.; Zhou, R.; Chai, Z.; Wang, S. Mechanism Unravelling for Ultrafast and Selective $^{99}TcO_4^-$ Uptake by a Radiation-Resistant Cationic Covalent Organic Framework: A Combined Radiological Experiment and Molecular Dynamics Simulation Study. *Chem. Sci.* **2019**, *10*, 4293-4305.

[16] Liu, Z.-W.; Han, B.-H. Evaluation of an Imidazolium-Based Porous Organic Polymer as Radioactive Waste Scavenger. *Environ. Sci. Technol.* **2020**, *54*, 216-224.

[17] Fei, H. H.; Bresler, M. R.; Oliver, S. R. J. A New Paradigm for Anion Trapping in High Capacity and Selectivity: Crystal-to-Crystal Transformation of Cationic Materials. *J. Am. Chem. Soc.* **2011**, *133*, 11110-11113.

[18] Li, C. P.; Ai, J. Y.; Zhou, H.; Chen, Q.; Yang, Y. J.; He, H. M.; Du, M. Ultra-Highly Selective Trapping of Perrhenate/Pertechnetate by a Flexible Cationic Coordination Framework. *Chem. Commun.* **2019**, *55*, 1841-1844.

[19] Sheng, D.; Zhu, L.; Dai, X.; Xu, C.; Li, P.; Pearce, C. I.; Xiao, C.; Chen, J.; Zhou, R.; Duan, T.; Farha, O. K.; Chai, Z.; Wang, S. Successful Decontamination of $^{99}TcO_4^-$ in Groundwater at Legacy Nuclear Sites by a Cationic Metal–Organic Framework with Hydrophobic Pockets. *Angew. Chem., Int. Ed.* **2019**, *58*, 4968-4972.

[20] Li, C. P.; Zhou, H.; Wang, J. J.; Liu, B. L.; Wang, S.; Yang, X.; Wang, Z. L.; Liu, C. S.; Du, M.; Zhou, W. Z. Mechanism-Property Correlation in Coordination Polymer Crystals toward Design of a Superior Sorbent. *ACS Appl. Mater. Interfaces* **2019**, *11*, 42375-42384.

[21] Karmakar, A.; Desai, A. V.; Ghosh, S. K. Ionic Metal–Organic Frameworks (IMOFs): Design Principles and Applications. *Coord. Chem. Rev.* **2016**, *307*, 313-341.

[22] Zhao, J.; Wang, Y. N.; Dong, W. W.; Wu, Y. P.; Li, D. S.; Liu, B.; Zhang, Q. A New Surfactant-Introduction Strategy for Separating the Pure Single-Phase of Metal–Organic Frameworks. *Chem. Commun.* **2015**, *51*, 9479-9482.

[23] Li, C. P.; Zhou, H.; Wang, S.; Chen, J.; Wang, Z. L.; Du, M. Highly Efficient $Cr_2O_7^{2-}$ Removal of a 3D Metal–Organic Framework Fabricated by Tandem Single-Crystal to Single-Crystal Transformations from a 1D Coordination Array. *Chem. Commun.* **2017**, *53*, 9206-9209.

[24] Fu, H. R.; Wang, N.; Qin, J. H.; Han, M. L.; Ma, L. F.; Wang, F. Spatial Confinement of a Cationic MOF: A SC-SC Approach for High Capacity Cr(VI)-Oxyanion Capture in Aqueous Solution. *Chem. Commun.* **2018**, *54*, 11645-11648.

[25] Zhu, L.; Sheng, D.; Xu, C.; Dai, X.; Silver, M. A.; Li, J.; Li, P.; Wang, Y.; Wang, Y.; Chen, L.; Xiao, C.; Chen, J.; Zhou, R.; Zhang, C.; Farha, O. K.; Chai, Z.; Albrecht-Schmitt, T. E.; Wang, S. Identifying the Recognition Site for Selective Trapping of $^{99}TcO_4^-$ in a Hydrolytically Stable and Radiation Resistant Cationic Metal–Organic Framework. *J. Am. Chem. Soc.* **2017**, *139*, 14873-14876.

[26] Sheng, D.; Zhu, L.; Xu, C.; Xiao, C.; Wang, Y.; Wang, Y.; Chen, L.; Diwu, J.; Chen, J.; Chai, Z.; Albrecht-Schmitt, T. E.; Wang, S. Efficient and Selective Uptake of TcO_4^- by a Cationic Metal–Organic Framework Material with Open Ag^+ Sites. *Environ. Sci. Technol.* **2017**, *51*, 3471-3479.

[27] Phelps, T. E.; Bhawawet, N.; Jurisson, S. S.; Baker, G. A. Efficient and Selective Extraction of $^{99m}TcO_4^-$ from Aqueous Media Using Hydrophobic Deep Eutectic Solvents. *ACS Sustain. Chem. Eng.* **2018**, *6*, 13656-13661.

[28] Chatterjee, S.; Norton, A. E.; Edwards, M. K.; Peterson, J. M.; Taylor, S. D.; Bryan, S. A.; Andersen, A.; Govind, N.; Albrecht-Schmitt, T. E.; Connick, W. B.; Levitskaia, T. G. Highly Selective Colorimetric and Luminescence Response of a Square-Planar Platinum(II) Terpyridyl Complex to Aqueous TcO_4^-. *Inorg. Chem.* **2015**, *54*, 9914-9923.

[29] Desai, A. M.; Singh, P. K. Ratiometric Fluorescence Turn-On Sensing of Perrhenate Anion, a Non-Radioactive Surrogate of Hazardous Pertechnetate, in Aqueous Solution. *Sensor Actuat. B-Chem.* **2018**, *277*, 205-209.

[30] Amendola, V.; Bergamaschi, G.; Boiocchi, M.; Alberto, R.; Braband, H. Fluorescent Sensing of ^{99}Tc Pertechnetate in Water. *Chem. Sci.* **2014**, *5*, 1820-1826.

[31] Desai, A. M.; Singh, P. K. An Ultrafast Molecular-Rotor-Based Fluorescent Turn-On Sensor for the Perrhenate Anion in Aqueous Solution. *Chem. Eur. J.* **2019**, *25*, 2035-2042.

[32] Rapti, S.; Diamantis, S. A.; Dafnomili, A.; Pournara, A.; Skliri, E.; Armatas, G. S.; Tsipis, A. C.; Spanopoulos, I.; Malliakas, C. D.; Kanatzidis, M. G.; Plakatouras, J. C.; Noli, F.; Lazarides, T.; Manos, M. J. Exceptional TcO_4^- Sorption Capacity and Highly Efficient ReO_4^- Luminescence Sensing by Zr^{4+} MOFs. *J. Mater. Chem. A* **2018**, *6*, 20813-20821.

[33] Blöchl, P. E. Projector Augmented-Wave Method, *Phys. Rev. B* **1994**, *50*, 17953-17979.

[34] Kresse, G.; Joubert, D. From Ultrasoft Pseudopotentials to the Projector Augmented-Wave Method. *Phys. Rev. B* **1999**, *59*, 1758-1775.

[35] Kresse, G.; Hafner, J. *Ab initio* Molecular Dynamics for Liquid Metals. *Phys. Rev. B* **1993**, *47*, 558-561.

[36] Perdew, J. P.; Burke, K.; Ernzerhof, M. Generalized Gradient Approximation Made Simple. *Phys. Rev. Lett.* **1996**, *77*, 3865-3868.

[37] Grimme, S. Semiempirical GGA-Type Density Functional Constructed with a Long-Range Dispersion Correction. *J. Comput. Chem.* **2006**, *27*, 1787-1799.

[38] Monkhorst, H. J.; Pack, J. D. Special Points for Brillouin-Zone Integrations. *Phys. Rev. B* **1976**, *13*, 5188-5192.

[39] Shao, Z.; Huang, C.; Wu, Q.; Zhao, Y.; Xu, W.; Liu, Y.; Dang, J.; Hou, H. Ion Exchange Collaborating Coordination Substitution: More Efficient Cr(VI) Removal Performance of a Water-stable Cu^{II}-MOF Material. *J. Hazard. Mater.* **2019**, *378*, 120719.

[40] Li, B.; Zhang, Y.; Ma, D.; Shi, Z.; Ma, S. Mercury Nano-Trap for Effective and Efficient Removal of Mercury(II) from Aqueous Solution. *Nat. Commun.* **2014**, *5*, 5537.

[41] Li, D.; Seaman, J. C.; Kaplan, D. I.; Heald, S. M.; Sun, C. J. Pertechnetate (TcO_4^-) Sequestration from Groundwater by Cost-Effective Organoclays and Granular Activated Carbon under Oxic Environmental Conditions. *Chem. Eng. J.* **2019**, *360*, 1-9.

[42] Xu, W.; Shao, Z.; Huang, C.; Xu, R.; Dong, B.; Hou, H. Alkenone-enol-alkenone [2+2+2] Cyclotrimerization Producing Functional Coordination Polymers with Excellent Adsorption Performance. *Inorg. Chem.* **2019**, *58*, 3959-3967.

[43] Li, C. P.; Chen, J.; Liu, C. S.; Du, M. Dynamic Structural Transformations of Coordination Supramolecular Systems upon Exogenous Stimulation. *Chem. Commun.* **2015**, *51*, 2768-2781.

[44] Schulz, W. W.; Lombardo, N. J. *Science and Technology for Disposal of Radioactive Tank Wastes*; Plenum Press: New York, USA, 1998.

[45] Xiao, C.; Khayambashi, A.; Wang, S. Separation and Remediation of $^{99}TcO_4^-$ from Aqueous Solutions. *Chem. Mater.* **2019**, *31*, 3863-3877.

[46] Cui, Y.; Yue, Y.; Qian, G.; Chen, B. Luminescent Functional Metal–Organic Frameworks. *Chem. Rev.* **2012**, *112*, 1126-1162.

[47] He, L.; Liu, C.; Xin, J. H. A Novel Turn-On Colorimetric and Fluorescent Sensor for Fe^{3+} and Al^{3+} with Solvent-Dependent Binding Properties and Its Sequential Response to Carbonate. *Sensor Actuat. B-Chem.* **2015**, *213*, 181-187.

[48] Sun, N. N.; Yan, B. Rapid and Facile Ratiometric Detection of CO_3^{2-} Based on Heterobimetallic Metal–Organic Frameworks (Eu/Pt-MOFs). *Dye Pigments* **2017**, *142*, 1-7.

[49] Li, C. P.; Ai, J. Y.; He, H. M.; Li, M. Z.; Du, M. Divergent Structural Transformations in 3D Ag(I) Porous Coordination Polymers Induced by Solvent and Anion Exchanges. *Cryst. Growth Des.* **2019**, *19*, 2235-2244.

[50] Karmakar, A.; Samanta, P.; Dutta, S.; Ghosh, S. K. Fluorescent "Turn-on" Sensing Based on Metal–Organic Frameworks (MOFs). *Chem. Asian J.* **2019**, *20*, 4506-4519.

[51] Chang, Y. C.; Wang, S. L. From Stimuli-Responsive Polymorphic Organic Dye Crystals to Photoluminescent Cationic Open-Framework Metal Phosphate. *J. Am. Chem. Soc.* **2012**, *134*, 9848-9851.

[52] Fu, H. R.; Wu, X. X.; Ma, L. F.; Wang, F.; Zhang, J. Dual-Emission SG7@MOF Sensor via SC-SC Transformation: Enhancing the Formation of Excimer Emission and the Range and Sensitivity of Detection. *ACS Appl. Mater. Interfaces* **2018**, *10*, 18012-18020.

[53] Chen, S.; Shi, Z.; Qin, L.; Jia, H.; Zheng, H. Two New Luminescent Cd(II)-Metal–Organic Frameworks as Bifunctional Chemosensors for Detection of Cations Fe^{3+}, Anions CrO_4^{2-}, and $Cr_2O_7^{2-}$ in Aqueous Solution. *Cryst. Growth Des.* **2017**, *17*, 67-72.

[54] Liu, W.; Wang, Y.; Bai, Z.; Li, Y.; Wang, Y.; Chen, L.; Xu, L.; Diwu, J.; Chai, Z.; Wang, S. Hydrolytically Stable Luminescent Cationic Metal Organic Framework for Highly Sensitive and Selective Sensing of Chromate Anions in Natural Water Systems. *ACS Appl. Mater. Interfaces* **2017**, *9*, 16448-16457.

[55] Chatterjee, S.; Bryan, S. A.; Seliskar, C. J.; Heineman, W. R. Three-Component Spectroelectrochemical Sensor Module for the Detection of Pertechnetate (TcO_4^-). *Rev. Anal. Chem.* **2013**, *32*, 209-224.

Table of Contents